Bionatura
Latin American Journal of Biotechnology and Life Sciences

Bionatura Issue 4 Vol 8 No 1 2023

Article

Molecular Docking, Design, Synthesis, Characterization and Pharmacological Evaluation of New 2-hydrazinel Oxazole containing moiety as anti-proliferative activity

Ayat K. Abdulellah[1,], Monther F. Mahdi[1], and Ayad M.R. Raauf[1]*
[1]Department of Pharmaceutical Chemistry, College of Pharmacy, Mustansiriyah University, Baghdad, Iraq.
* *Correspondence: Aeyatkhalid@gmail.com*
Available from: http://dx.doi.org/10.21931/RB/CSS/2023.08.04.10

ABSTRACT
A new series of 1,3-oxazole attached to bromonabumetone derivatives have been designed and in silico studying as molecular docking using (GOLD) suite program and determination of pharmacokinetic properties using Swiss ADME suite, and then best fitting compounds were synthesized successfully, and confirmed using spectral analysis FT-IR, ^{1}HNMR and ^{13}CNMR. In vitro evaluation as an anti-proliferative activity for epidermal growth factor receptor (EGFR) Tyrosine kinase using MTT assay. The anti-proliferative investigation revealed a dose-dependent impact on lung cancer cells (A549) with inhibitory concentration IC_{50} for compounds 4b and 4c (6.14 & 14.8) µM, respectively which was significantly higher than that of erlotininb IC_{50} = 24.6 µM. While compound 4a had IC_{50} (26.8) µM, which is closely related to erlotininb.
Keywords: 1,3-Oxazole, EGFR, nabumetone, A549 cell line, molecular docking, pharmacokinetic study

INTRODUCTION

Cancer has been classified as one of the leading life-threatening causes worldwide owing to its massive and complicated etiology [1]. Cancer is a lethal disease, especially in developed countries. In 2030, it is expected that the mortality rate will be increased to 13.1 million deaths [2].

Several kinases function as an on/off switch for cellular motility and proliferation. Thus, mutations of these kinases are responsible for cellular irregularities affording cancer initiation, metastasis or progression [3]. One of the most prominent oncogenic kinases is epidermal growth factor receptor (EGFR), which is overexpressed in a multiplicity of human cancers, including breast, colorectal, lung, prostate, ovary and pancreatic cancer [4]. Poor treatment outcomes due to resistance to radiotherapy, hormone therapy, and cytotoxic drugs presented an opportunity for anti-EGFR drug recommendations due to their higher safety and efficacy compared to standard chemotherapy [5&6]. Accordingly, the inhibition of tyrosine kinase activity has provided a rational approach to cancer therapy by discovering newly synthesized anti-neoplastic compounds or the structural manipulations of already-known molecular cores [7].

Many heterocyclic compounds are very important in medicinal chemistry since they exhibit remarkable and various pharmacological activities [8]. Among them, the synthetic heterocyclic containing oxazole nucleus has a wide range of pharmacological activities that emerged in the last 20 years [9]. These include antifungal, antiparasitic, and anti-inflammatory activities and the most important anticancer activities, Such as mubritinib, a tyrosine kinase inhibitor [10, 11, 12, 13]. Furthermore, many of the literature syntheses of new compounds containing oxazole nuclei gave interest activity against lung cancer cell line A549 targeted EGFR tyrosine kinase, as shown in figure (1).

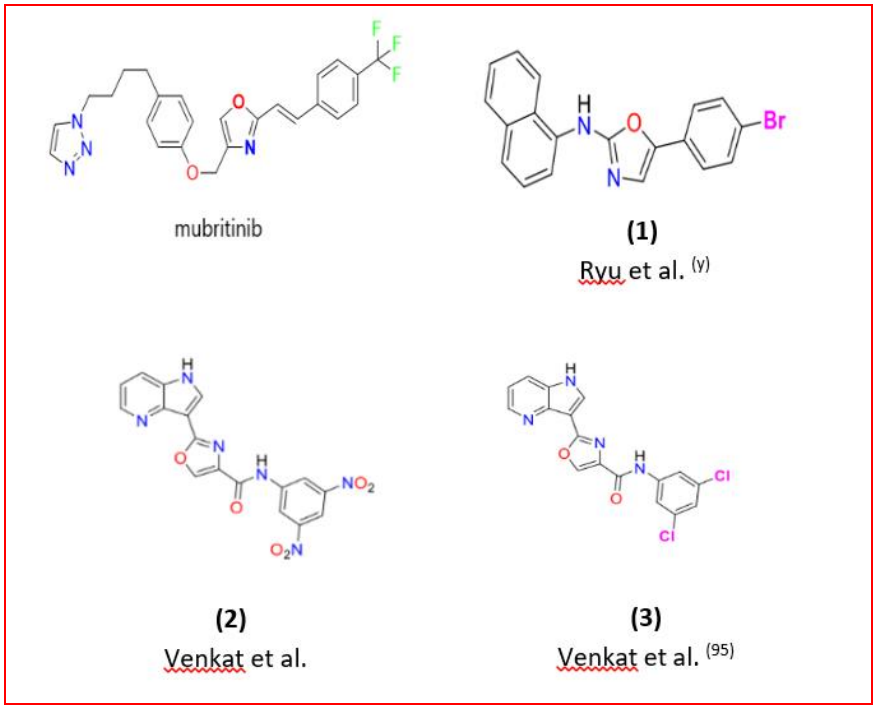

Figure 1. Structures of some representative pharmacologically active compounds contain oxazole nucleus

Molecular docking is one of the most common technologies used in structure-based drug design (SBDD) due to its great ability to accurately forecast the chemical structure of small molecule ligands within the appropriate target binding location, as shown in Figure (2) [16]. The use of molecular docking in drug discovery has become crucial [17]. By ranking docked molecules according to how efficiently they bind ligand-receptor complexes [18].

Our findings showed that 1,3-oxazole-based compounds could be potent agents regarding anticancer activity, but the real challenge for chemists and oncologists with cancer chemotherapy and antitumor agents. This is due to many anticancer agents' non-selectivity, acute toxicity, and cellular drug resistance. So, there is a continuing need for designing and developing new chemotherapeutic agents for cancer treatment [19].

So, in an attempt to develop new anticancer agents targeted EGFR, our group devoted considerable interest to synthesizing compounds based on the oxazole ring as the pharmacophore center. This study evaluated the anticancer effects of 4 compounds (4a–d) from the classes mentioned above in vitro against a lung

cancer cell line (A549). In silico prediction of EGFR tyrosine kinase inhibition and pharmacokinetics of the tested compounds was also performed.

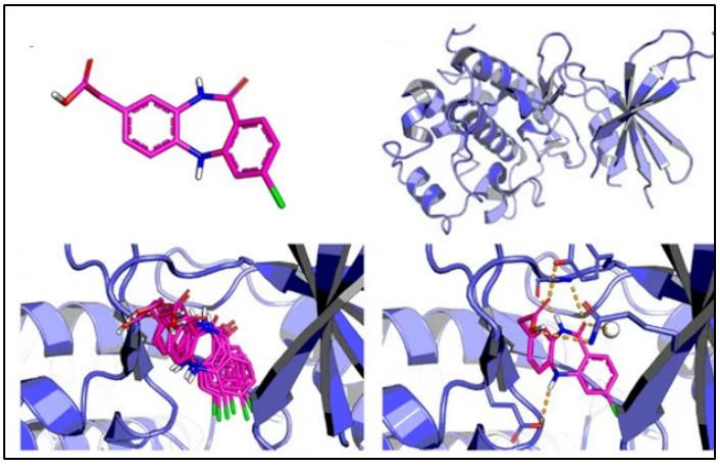

Figure 2. Overall process of prediction in molecular docking

MATERIALS AND METHODS

All intermediates were purchased from Sigma Aldrich, USA and hyper-chem, Hangxing RD., Hangzhou, China. While melting point was recorded by capillary tube method on an electric melting point instrument from England Stuart Company, instrumentation ^{1}H NMR and ^{13}C NMR with quality 500 & 125 MHz, respectively, with Varian / Aligent USA Company, and FT-IR on Shimazu 8400s from Japan

Chemical synthesis:

In the scheme below, some new Oxazole derivatives were synthesized using the following procedures illustrated in (Figure 3).

Procedure for the synthesis of 1-bromo-4-(6-methoxynaphthalen-2-yl) butan-2-one (1):

To a well-stirred solution of nabumetone (0.912 g, 4.0 mmol) in dioxane/diethyl ether mixture (1:2) (48 mL), the bromine (0.623 mL, 4.0 mmol) was added dropwise with constant stirring. After 4 hours, the reaction blend was poured into 10 mL of cold water, and then the isolated product was filtered off and recrystallized from ethanol to obtain (1) [(20)].

Procedure for the synthesis of semicarbazone derivatives (3a-d):

The aqueous solution of semicarbazide hydrochloride (20 mL) (1.110g, 1.0 mmol) was added dropwise to a hot aqueous solution of different acetyl pyridine (20 mL) (a-d) (1.0 mmol) when sodium acetate is existence (0.829 g, 1.0 mmol). For 2 hours, the reaction mixture was stirred. The solid was filtered off, washed, dried, and recrystallized using EtOH to afford (3a-d) [(21)].

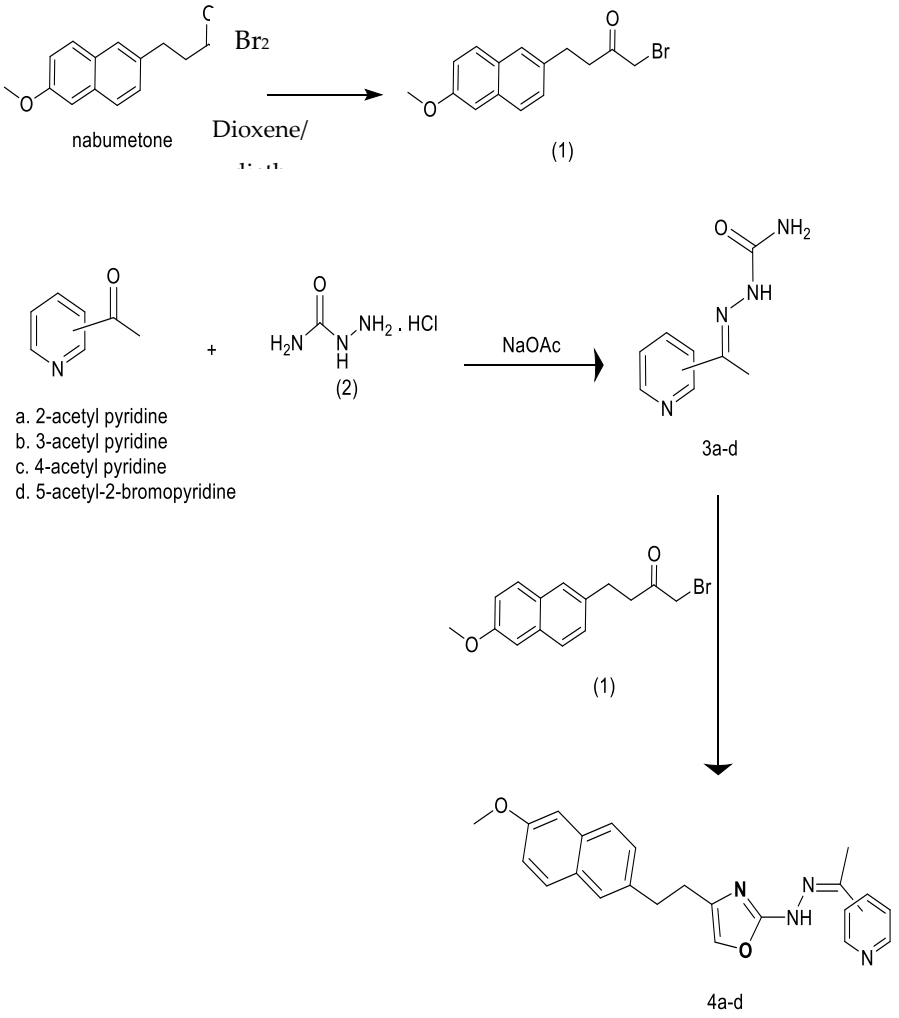

Figure 3. Synthesis final compounds (4a-d)

Procedure for the synthesis of oxazole derivatives (4a-d):

The appropriate bromonabumetone (1) (4.0 mmol) was introduced to a semicarbazone derivative (3a-d) (4.0 mmol) in EtOH (80 mL). After 24 hours of stirring at room temperature, the resulting solid was filtered, washed with ethanol, dried, and recrystallized with EtOH to yield (4a-d) [(22)].

(E)-2-(1-(pyridin-2-yl)ethylidene)hydrazine-1-carboxamide (3a):

White crystal, mp 198-200 °C, yield 95%, IR υmax: 3405.84 & 3369.80 cm^{-1} (NH_2), 3191.04 cm^{-1} (NH), 3065.48 cm^{-1} (aromatic C-H), 2911.94 cm^{-1} (CH_3), 1686.51 cm^{-1} (C=O), 1581.66 cm^{-1} (C=N), 1568.15 cm^{-1} (C=C of aromatic); ^{1}H NMR (500 MHz, DMSO, δ): 2.25 (3H, s, CH_3), 6.63 (2H, s, NH_2), 7.30 – 8.53 (4H, m, Ar-H), 9.52 (1H, s, NH); ^{13}C NMR (DMSO-d6, ppm, 125 MHz): 11.93 (CH_3), 120.66 – 136.72 (3C of aromatic ring), 145.20 (C=N), 148.66- 155.65 (2C of aromatic ring), 157.46 (C=O).

(E)-2-(1-(pyridin-3-yl)ethylidene)hydrazine-1-carboxamide (3b):

White crystal, mp 211-213 °C, yield 85%, IR υmax: 3423.77 & 3211.76 cm^{-1} (NH_2), 3186.65 cm^{-1} (NH), 3076.63 cm^{-1} (aromatic C-H), 2941.43 cm^{-1}

(CH_3), 1689.15 cm^{-1} (C=O), 1582.82 cm^{-1} (C=N), 1475.13 cm^{-1} (C=C of aromatic); ^1H NMR (500 MHz, DMSO, δ): 2.20 (3H, s, CH_3), 6.60 (2H, s, NH_2), 7.35 – 9.02 (4H, m, Ar-H), 9.51 (1H, s, NH); ^{13}C NMR (DMSO-d6, ppm, 125 MHz): 13.49 (CH_3), 123.66 – 147.71 (5C of aromatic ring), 149.54 (C=N), 157.71 (C=O).

(E)-2-(1-(pyridin-4-yl)ethylidene)hydrazine-1-carboxamide (3c):

White crystal, mp 209-211 °C, yield 93%, IR υmax: 3419.14 & 3241.08 cm^{-1} (NH_2), 3192.43 cm^{-1} (NH), 3079.79 cm^{-1} (aromatic C-H), 2959.04 cm^{-1} (CH_3), 1673.14 cm^{-1} (C=O), 1576.77 cm^{-1} (C=N), 1541.08 cm^{-1} (C=C of aromatic); ^1H NMR (500 MHz, DMSO, δ): 2.20 (3H, s, CH_3), 6.78 (2H, s, NH_2), 8.10 – 8.68 (4H, m, Ar-H), 9.88 (1H, s, NH); ^{13}C NMR (DMSO-d6, ppm, 125 MHz): 12.99 (CH_3), 121.92 – 145.81 (3C of aromatic ring), 145.81 (C=N), 149.92 (2C of aromatic), 157.12 (C=O).

(E)-2-(1-(6-bromopyridin-3-yl)ethylidene)hydrazine-1-carboxamide (3d):

Vegas gold crystal, mp 223-224 °C, yield 90%, IR υmax: 3492.32 & 3282.94 cm^{-1} (NH_2), 3201.03 cm^{-1} (NH), 3077.39 cm^{-1} (aromatic C-H), 2887.19 cm^{-1} (CH_3), 1690.39 cm^{-1} (C=O), 1584.55 cm^{-1} (C=N), 1577.46 cm^{-1} (C=C of aromatic), 831.72 cm^{-1} (C-Br); ^1H NMR (500 MHz, DMSO, δ): 2.17 (3H, s, CH_3), 6.62 (2H, s, NH_2), 7.58- 8.80 (4H, m, Ar-H), 9.55 (1H, s, NH); ^{13}C NMR (DMSO-d6, ppm, 125 MHz): 13.36 (CH_3), 127.84 – 141.35 (5 C of aromatic ring), 148.49 (C=N), 157.56 (C=O).

(Z)-4-(2-(6-methoxynaphthalen-2-yl)ethyl)-2-(2-(1-(pyridin-2-yl) ethylidene) hydrazineyl) oxazole (4a):

Pale brown powder, mp 119-120 °C, yield 72%, IR υmax: 3267.89 cm^{-1} (NH), 3000.60 cm^{-1} (aromatic C-H), 2929.54 cm^{-1} (CH_3), 1635.69 cm^{-1} (C=N of imine), 1599.17 cm^{-1} (C=N of imine), 1491.14 cm^{-1} (C=C of aromatic); ^1H NMR (500 MHz, DMSO, δ): 2.25 (3H, s, CH_3), 2.80 (2H, t, CH_2-CH_2), 2.86 (2H, t, CH_2-CH_2), 3.84 (3H, s, OCH_3), 7.09 – 7.75 (7H, m, Ar-H), 7.76 (1H, s, CH of oxazole), 8.28- 8.53 (3H, m, Ar-H), 9.49 (1H, s, NH); ^{13}C NMR (DMSO-d6, ppm, 125 MHz): 11.91 (CH_3), 29.51 (CH_2 next to oxazole), 30.23 (CH_2 next to aromatic ring), 55.57 (CH_3-O-C), 106.22 – 120.63 (3 C of aromatic ring), 123.67 (C-4, oxazole), 126.30- 136.66 (9 C of aromatic ring), 138.34 (C-2, Oxazole), 145.61 (C=N of hydrazine), 148.68- 154.16(2 C of aromatic ring), 155.91 (C-5, Oxazole), 157.41 (C-O-CH_3).

(Z)-4-(2-(6-methoxynaphthalen-2-yl)ethyl)-2-(2-(1-(pyridin-3-yl) ethylidene) hydrazineyl) oxazole (4b):

Pale gold powder, mp 260-261 °C, yield 82%, IR υmax: 3246.64 cm^{-1} (NH), 3045.11 cm^{-1} (aromatic C-H), 2952.06 cm^{-1} (CH_3), 1645.93 cm^{-1} (C=N of oxazole), 1615.40 cm^{-1} (C=N of imine), 1515.12 cm^{-1} (C=C of aromatic); ^1H NMR (500 MHz, DMSO, δ): 2.33 (3H, s, CH_3), 2.86 (2H, t, CH_2-CH_2), 3.04 (2H, t, CH_2-CH_2), 3.80 (3H, s, OCH_3), 7.06 – 7.69 (7H, m, Ar-H), 7.74 (1H, s, CH of oxazole), 7.89 – 9.32 (4H, m, Ar-H), 10.46 (1H, s, NH); ^{13}C NMR (DMSO-d6, ppm, 125 MHz): 24.02 (CH_3), 33.16 (CH_2 next to oxazole), 36.93 (CH_2 next to aromatic ring), 53.98 (CH_3-O-C), 105.79 – 123.68 (3 C of aromatic ring), 125.36 (C-4, oxazole), 125.60- 138.32 (9 C of aromatic ring), 139.31 (C-2, Oxazole), 147.46 (C-5, oxazole), 150.95-151.51 (2 C of aromatic ring), 154.16 (C-O-CH_3), 169.89 (C=N of hydrazone).

(Z)-4-(2-(6-methoxynaphthalen-2-yl)ethyl)-2-(2-(1-(pyridin-4-yl) ethylidene) hydrazineyl) oxazole (4c):

White powder, mp 168-170 °C, yield 84%, IR υmax: 3306.78 cm^{-1} (NH), 3030.70 cm^{-1} (aromatic C-H), 2962.13 cm^{-1} (CH_3), 1640.02 cm^{-1} (C=N of oxazole), 1603.74 cm^{-1} (C=N of imine), 1554. 75 cm^{-1} (C=C of aromatic); ^1H

NMR (500 MHz, DMSO, δ): 2.10 (3H, s, CH_3), 2.81 (2H, t, CH_2-CH_2), 2.88 (2H, t, CH_2-CH_2), 3.83 (3H, s, OCH_3), 7.09 – 7.71 (7H, m, Ar-H), 7.72 (1H, s, CH of oxazole), 7.74 – 8.58 (3H, m, Ar-H), 10.42 (1H, s, NH); ^{13}C NMR (DMSO-d6, ppm, 125 MHz): 22.46 (CH_3), 29.50 (CH_2 next to oxazole), 30.23 (CH_2 next to aromatic ring), 55.57 (CH_3-O-C), 106.22 – 124.17 (4 C of aromatic ring), 126.30 (C-4, oxazole), 127.14- 133.48 (7 C of aromatic ring), 136.72 (C-2, Oxazole), 140.21-148.56 (3 C of aromatic ring), 151.54 (C-5, oxazole), 157.30 (C-O-CH_3), 164.70 (C=N of hydrazone).

(Z)-2-(2-(1-(6-bromopyridin-3-yl)ethylidene)hydrazineyl)-4-(2-(6-methoxynaphthalen-2-yl)ethyl)oxazole (4d):

Brown powder, mp 140-142°C, yield 80%, IR υmax: 3206.46 cm^{-1} (NH), 3021.84 cm^{-1} (aromatic C-H), 2818.88 cm^{-1} (CH_3), 1646.56 cm^{-1} (C=N of oxazole), 1608.64 cm^{-1} (C=N of imine), 1577.38 cm^{-1} (C=C of aromatic), 832.73 cm^{-1} (C-Br); ^{1}H NMR (500 MHz, DMSO, δ): 2.10 (3H, s, CH_3), 2.80 (2H, t, CH_2-CH_2), 2.86 (2H, t, CH_2-CH_2), 3.83 (3H, s, OCH_3), 7.09 – 7.71 (7H, m, Ar-H), 7.72 (1H, s, CH of oxazole), 7.89 – 8.81 (3H, m, Ar-H), 10.78 (1H, s, NH); ^{13}C NMR (DMSO-d6, ppm, 125 MHz): 19.60 (CH_3), 29.53 (CH_2 next to oxazole), 30.24 (CH_2 next to aromatic ring), 55.57 (CH_3-O-C), 106.21 – 118.94 (2 C of aromatic ring), 126.30 (C-4, oxazole), 127.13- 136.80 (10 C of aromatic ring), 137.92 (C-2, Oxazole), 145.43(C-5, oxazole), 150.22-155.79 (2 C of aromatic ring), 157.25 (C-O-CH_3), 163.23 (C=N of hydrazone).

Computational methods:

The computational method of our compounds is shown in Figure (3). Molecular docking was conducted by CCDC GOLD, Hermes visualizer program (v. 2020.3), which visualizes proteins, ligands, hydrogen bond interaction, short contacts and bond length estimation. chembioOffice software (v. 19.1) was used to draw reference and compound structures. SwissADME server for predicting the pharmacokinetics of our synthesized compounds [23].

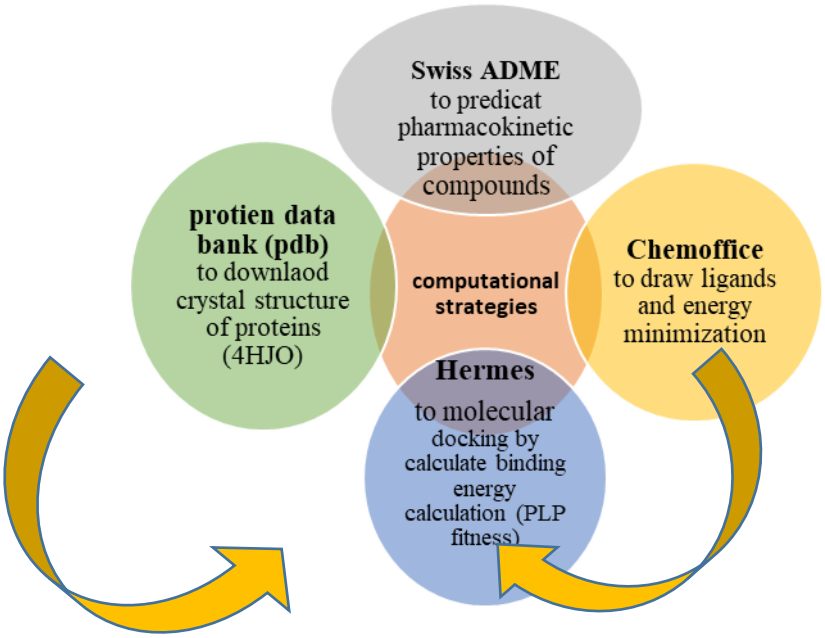

Figure 4. Computational protocol of the desired compounds

ADME procedures:

All ligands (4a-d) were drawn using Chem. axon and then converted by Swiss ADME tool to SMILE name to predict pharmacokinetic and physicochemical properties. The polarity and lipophilicity of the small molecule were determined by BOILED EGG [24].

Ligands and receptor Preparation:

The crystal structure of epidermal growth factor (EGFR) tyrosine kinase was obtained from the Protein Data Bank (PDB ID: 4HJO). The crystal structure of a protein is prepared in two steps: conserving water molecules involved in interaction and removing others and inserting hydrogen atoms to reach the amino acids residues' proper ionization and tautomeric state. The energy minimization of the synthesized ligands was accomplished using CheBio3D (v. 19.1) and the MM2 force field

Molecular Docking Protocol:

The molecular docking was performed by using the full license version of Genetic Optimization for Ligand Docking (GOLD) (v. 2020.3.0) [25]. The docking process is provided by using the Hermes visualizer program within GOLD. The binding site used in the docking was the protein residues and nucleotides within 10 A° of the reference ligands present in the complexes of protein structure. EGFR tyrosine kinase protein was downloaded from the PDB website (PDB: 4HJO) [26]. The protein reference ligand has been used to determine the active site radius (10 A°). Chemscore kinase was used as a configuration template. The scoring function was performed using PLP fitness. All parameters' values used in the GOLD docking process remained default, and all solutions were graded according to the Fitness function of Piecewise Linear Potential (CHEMPLP). The docking results, such as the docked pose, binding mode, and binding free energy, are used to assess the ligand's interaction with the protein residues of the active site of EGFR.

Cytotoxicity Assay:

The methodology used to investigate the anticancer activity of (4a-d) on the viability of lung cancer cell line (A549) by MTT assay [27]. This procedure was carried out at the College of Pharmacy/ Mustansiriyah University, Iraq.

Cell Culture and Maintenance

ATCC provided the lung cancer cell lines (A549). It was kept in the Tissue Culture Research Center's Cell Bank at Mustansiriyah University's College of Pharmacy. (A549) cells were cultured in RPMI-1640 media supplemented with 10% fetal bovine serum FBS and 1% L-Glutamine, as well as 1% Penicillin Streptomycin-Amphotericin B 100X as an antiseptic.

The Half Maximal Inhibitory Concentration (IC_{50}) Value Determination

According to the in vitro MTT experiment, the IC_{50} reflects the concentration of the chemicals tested (4a-d) that is necessary to decrease cell viability by 50%. The IC_{50} values for (4a-d) substances were determined using the in vitro MTT test 72 hours after the cells were exposed to these compounds. To compute the IC_{50}, plot the corrected absorbance at 520-600 nm (absorbance minus complete media) vs. the concentration of test compound (absorbance minus complete media) versus the concentration of test compound. [Inhibition Rate %= (A-B/A) * 100] was used to calculate the percent inhibition rate (percentage of

cytotoxicity) in a triplicate assay where A and B represent the optical densities of erlotinib (control) and test, respectively.

Statistical analysis

The nonlinear curve fitting program in GraphPad Prism was used to analyze the IC_{50} and MTT assay data of the tested compounds (4a-d) on A549 cells. A one-way ANOVA with Tukey test was utilized to compare all groups inside the same plate of MTT (prism and software). Statistical significance was defined as a value of $p > 0.05$.

RESULTS

ADME results interpretation:

a) ≤ 5 hydrogen bonds donor b) ≤10 hydrogen bond acceptor

c) Log P ≤ 5 d) Molecular weight (M.Wt) ≤500.

Furthermore, the topological polar surface area (TPSA) has been calculated, as it is a useful property related to the molecules' bioavailability. Passively absorbed compounds with a TPSA < 140 A^o are therefore believed to have high bioavailability; otherwise, this number means the compounds gave low bioavailability [30]. The ADME prediction data obtained showed that all compounds within the range of accepted values, these compounds have TPSA below 140 A^o. The bioavailability was 0.55 for all compounds, meaning they reached systemic circulation. Lipinski's rule of five (RO5) is shown in table (1). Also, all the derivatives fulfilled the topological descriptors and fingerprints of molecular drug-likeness structure keys as Log P and Log S.

Comp.	H-bond accep-tor	H-bo nd do-nor	MR	TPS A (A^o)	GI Abs	BBB permeant	Bioavailabil-ity	Lipinski violation
4a	5	1	114.84	72.54	High	NO	0.55	0
4b	5	1	114.84	72.54	High	NO	0.55	0
4c	5	1	114.84	72.54	High	NO	0.55	0
4d	5	1	122.54	72.54	High	NO	0.55	0

Table 1. ADME result of the final derivatives

Interpretation of docking results:

Energy minimization for ligands and the protein is needed to correct distorted geometries by moving atoms to release internal constraints. The geometry is repaired after reducing the energy, meaning a minimal amount of energy has been obtained.

In order to predict the selectivity and binding energies of the ligands for the target, the interactions between our ligands (4a-d) and the target in the modeled complexes were examined. They observed the fitness function ability of this complex by all desired compounds. The binding affinity of compounds (4a-d) and human estrogen receptors were ranked based on their average PLP fitness involved in the complex formation at the active sites. The PLP fitness of the docked compounds on the target was found in the range of 82.23 to 91.94 with their amino acid interactions as shown in table (2) and shown in figure (4 to 6). In our work, the synthesized ligands (4b & 4c) gave promising docking results with EGFR tyrosine kinase showed the best docking on PLP fitness (91.94 & 90.38), respectively. At the same time, compound (4a & 4d) had PLP fitness (85.16 & 82.23), respectively, closely related to erlotinib score with PLP fitness (85.42). Finally, there is a compatible correlation between our docking analysis and the experimental results.

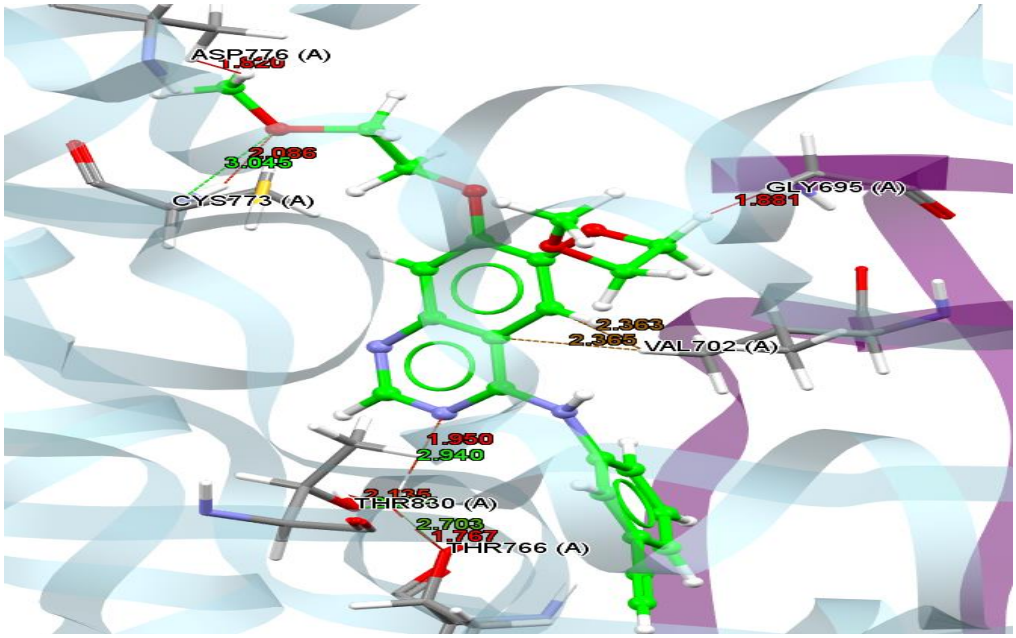

Figure 5. 3D structural image of H-bond (green color) and brief contact interaction (red color) profiles for erlotinib binding with EGFR (code of PDB: 4HJO). Erlotinib is administered in a ball-and-stick format, whereas amino acids are administered as capped sticks.

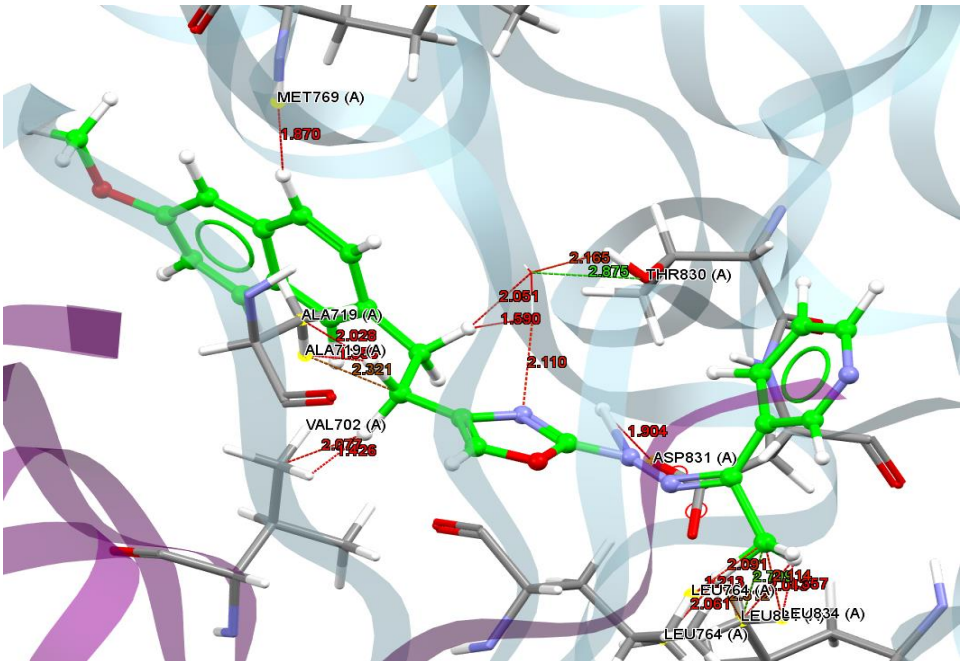

Figure 6. 3D structural image of H-bond (green color) and brief contact interaction (red color) profiles for compound 4b binding with EGFR (code of PDB: 4HJO). Compound 4b is administered in a ball-and-stick format, whereas amino acids are administered as capped sticks.

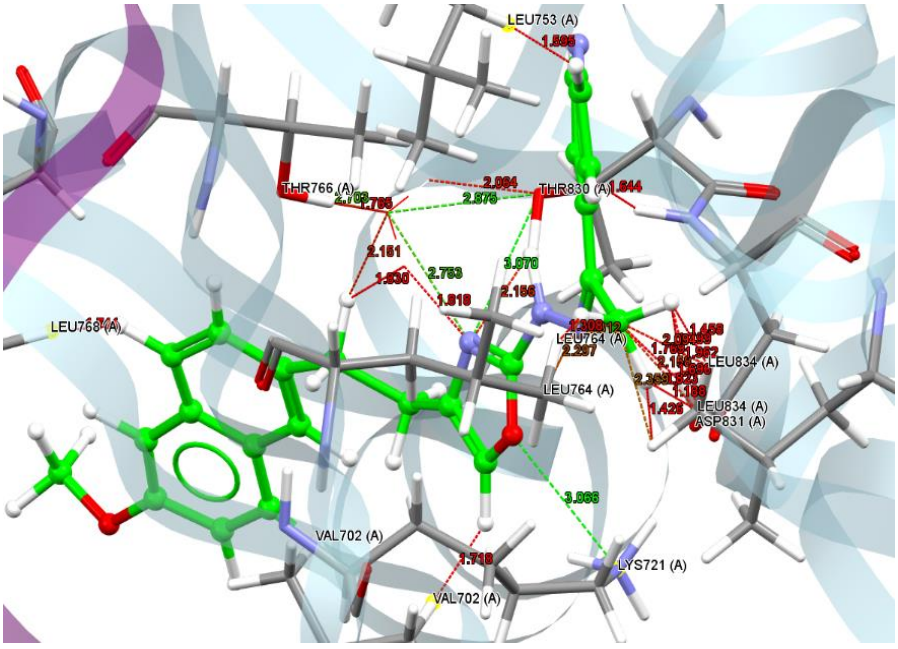

Figure 7. 3D structural image of H-bond (green color) and brief contact interaction (red color) profiles for compound 4c binding with EGFR (code of PDB: 4HJO). Compound 4c is administered in a ball-and-stick format, whereas amino acids are administered as capped sticks.

Protein data bank	Compounds	Binding Energy (PLP Fitness)	H-Bond interactions	Short contact interactions
			Amino acid residues	Amino acid residues
Epidermal Growth factor (EGFR) Tyrosine kinase code: (4HJO)	**4a**	85.16	ASP 831, THR 766, THR 830	CYS 751, THR 830, THR 766, ASP 831, LYS 721, VAL 702
	4b	91.94	LEU 834	MET 769, ASP 831, VAL 702 (2), ALA 719 (3), LEU 834 (4), LEU 764 (3), 3 HOH bridge with THR 830 & THR 766
	4c	90.38	LYS 721, THR 830, HOH bridge with THR 830 & THR 766	LEU 768, VAL 702, THR 830, HOH bridge with THR 830 & THR 766, LEU 753, ASP 831, LEU 834 (11), LEU 764
	4d	82.23	LEU 721, THR 766	LEU 768, ASP 831, LEU 834
	Erlotinib	85.42	CYS 773, HOH bridge with THR 830 & THR 766	GLY 695, CYS 773, HOH bridge with THR 830 & THR 766, ASP 776, VAL 702 (2)

Table 2. The binding energies for our final compounds Interpretation of anti-proliferative evaluation against lung cancer cell line.

Interpretation of anti-proliferative evaluation against breast cancer cell line

The anti-proliferative activity of synthesized compounds (4a-d) was demonstrated by MTT assay and represent in table (3) that demonstrate Compounds (4b & 4c) had the best and most potent anti-proliferative effect on A549 cell line, with an IC_{50} value of (6.14 & 14.8) µM respectively, compound 4b is about 4 times more active than erlotinib, while compound 4c about 1.7 times more than reference drug, which has an IC_{50} value of 24.6 µM, implying that compounds (4b & 4c) requires a lower concentration to inhibit cancerous A549 cell growth than erlotinib. On the other hand, compound 4a showed a closely related to erlotinib with IC_{50}. Figure 8 shows the dosage response curve of the IC_{50} value of erlotinib on A549, while Figures 10 to 11 show the dosage response curves of the IC50 value of our potent compounds.

Cell type	Compound 4a	Compound 4b	Compound 4c	Compound 4d	Erlotinib
A459	26.8 µM	6.14 µM	14.8 µM	77.5 µM	24.6 µM

Table 3. represents the IC_{50} of synthesized final compounds and erlotinib

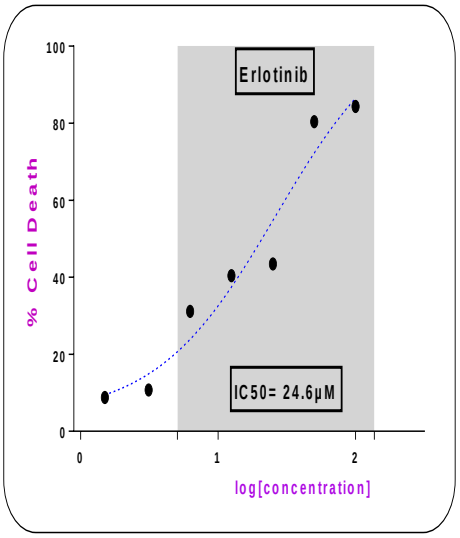

Figure 8. Dose-response curve of IC_{50} for Erlotinib on A549

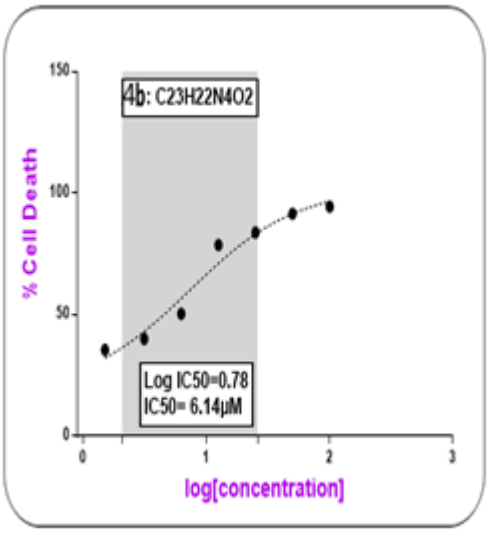

Figure 9. Dose-response curve of IC_{50} for compound (4b) on A549

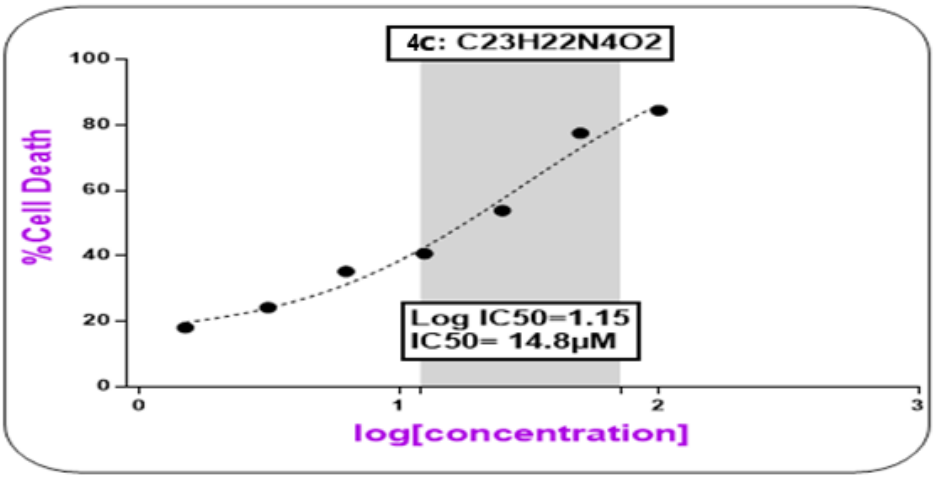

Figure 10. Dose-response curve of IC_{50} for compound (4c) on A549

DISCUSSION

The drug-like properties of our final compounds (4a-d) were calculated following Lipinski's rule of five [28]. This rule is also called Pfizer's rule of five (RO5). The method has been widely used as a screening for compounds that might potentially be used as a lead for drug discovery projects. In a sense, Lipinski's rule of five relates to the oral administration of medicines that must possess the following qualities to be administered orally [29].

All final synthesized compounds (4a-d) were successfully docked using the GOLD Suite program. The term "GOLD" refers to a "genetic strategy for docking flexible ligands into protein binding sites [31]. GOLD has been extensively validated and has shown superior posture prediction rendering and virtual screening outcomes [32]. This is included in the GOLD Suite, which includes additional software components such as Hermes, Mercury, Isostar, Conquest, and GoldMine.

CONCLUSION

The synthesis of designed compounds (4a-d) has been successfully achieved, and then evaluation gives anti-proliferative. The result of in vitro evaluation indicates that some compounds were strongly anti-proliferative against lung cancer cell line activity like compounds (4a, 4b & 4c) on A549. While compounds (4b & 4c) gave excellent anti-proliferative against EGFR tyrosine kinase cell line (A549), these results are consistent with the docking study on EGFR tyrosine kinase comparable with erlotinib. Additionally, the ADME evaluation showed that all synthesized compounds fulfilled the Lipinski rule.

Credit authorship contribution statement

Aeyat K. Abdulellah: conceptualization, data curation, investigation, methodology, software, supervision, Monther F. Mahdi: validation, writing-review & editing. Ayad M.R. Raauf: Visualization, writing- original draft, writing-review & editing

The authors declare no conflict of interest.

Acknowledgments

The authors are grateful to the chairman and members of the Department of Pharmaceutical Chemistry, college of Pharmacy, Mustansiriyah University, for their help and support.

Reference

1 A. Irfan, F. Batool, S.A.Z. Naqvi, A. Islam, S.M. Osman, A. Nocentini, S.A. Alissa, C. T. Supuran, Benzothiazole derivatives as anticancer agents, J. Enzym. Inhib. Med. Ch. 35 (1) (**2020**) 265–279.

2 19-Labib MB, Philoppes JN, Lamie PF, Ahmed ER. Azole-hydrazone derivatives: Design, synthesis, in vitro pharmacological evaluation, dual EGFR/HER2 inhibitory activity, cell cycle analysis and molecular docking study as anticancer agents. Bioorganic chemistry. **2018** Feb 1;76:67-80.

3 Du, Z.; Lovly, C.M. Mechanisms of receptor tyrosine kinase activation in cancer. Mol. Cancer **2018**, 17, 58.

4 Khattab, RR; Hassan, A.A.; Osman, D.A.A.; Abdel-Megeid, F.M.; Awad, H.M.; Nossier, E.S.; El-Sayed, W.A. Synthesis, anticancer activity and molecular docking of new triazolo [4,5-d] pyrimidines based thienopyrimidine system and their derived N-glycosides and thioglycosides. Nucleosides Nucleotides Nucleic Acids **2021**, 40, 1090–1113.

5 Khattab, RR; Alshamari, A.K.; Hassan, A.A.; Elganzory, H.H.; El-Sayed, W.A.; Awad, H.M.; Nossier, E.S.; Hassan, N.A. Click chemistry-based synthesis, cytotoxic activity and molecular docking of novel triazole-thienopyridine hybrid glycosides targeting EGFR. J. Enzym. Inhib. Med. Chem. **2021**, 36, 504–516.

6 Othman, I.M.; Alamshany, Z.M.; Tashkandi, N.Y.; Gad-Elkareem, M.A.; Anwar, M.M.; Nossier, E.S. New pyrimidine and pyrazole-based compounds as potential EGFR inhibitors: Synthesis, anticancer, antimicrobial evaluation and computational studies. Bioorg. Chem. **2021**, 114, 105078.

7 Amin NH, Elsaadi MT, Zaki SS, Abdel-Rahman HM. Design, synthesis and molecular modeling studies of 2-styrylquinazoline derivatives as EGFR inhibitors and apoptosis inducers. Bioorganic Chemistry. **2020** Dec 1;105:104358.

8 Ghanim ZS, Mahdi MF, Raauf AM. Molecular docking, synthesis, anticancer assessment and ADME study of naproxen containing imidazole ring derivatives. Materials Today: Proceedings. **2021** Jun 5.

9 El-Nezhawy, A. O. H., Eweas, A. F., Radwan, M. A. A., & El-Naggar, T. B. A. (**2015**). Synthesis and Molecular Docking Studies of Novel 2-Phenyl-4-Substituted Oxazole Derivatives as Potential Anticancer Agents. Journal of Heterocyclic Chemistry, 53(1), 271–279. doi:10.1002/jhet.2422

10 10- Sharma, V.; Bhatia, P.; Alam, O.; Javed Naim, M.; Nawaz, F.; Ahmad Sheikh, A.; Jha, M. Recent advancement in the discovery and development of COX-2 inhibitors: Insight into pharmacological activities and SAR studies (2008–2019). Bioorg. Chem. 2019, 89, 103007.

11 Guerrero-Pepinosa, N.Y.; Cardona-Trujillo, M.C.; Garzón-Castaño, S.C.; Veloza, L.A.; Sepúlveda-Arias, J.C. Anti-proliferative activity of thiazole and oxazole derivatives: A systematic review of in vitro and in vivo studies. Biomed. Pharmacother. 2021, 138, 111495.

12 Yan, X.; Wen, J.; Zhou, L.; Fan, L.; Wang, X.; Xu, Z. Current Scenario of 1,3-oxazole Derivatives for Anticancer Activity. Curr. Top. Med. Chem. **2020**, 20, 1916–1937.

13 Z. Yan, A. Liu, Y. Ou, J. Li, H. Yi, N. Zhang, M. Liu, L. Huang, J. Ren, W. Liu, A. Hu, Design, synthesis and fungicidal activity evaluation of novel pyrimidinamine derivatives containing phenyl-thiazole/oxazole moiety, Bioorg. Med. Chem. 27 (**2019**) 3218–3228.

14 Ryu H, Choi HK, Kim HJ, Kim AY, Song JY, Hwang SG, Kim JS, Kim DU, Kim EH, Kim J, Ahn J. Antitumor activity of a novel tyrosine kinase inhibitor AIU2001 due to abrogation of the DNA damage repair in non-small cell lung cancer cells. International journal of molecular sciences. **2019** Sep 24;20(19):4728.

15 Venkat Swamy P, Kiran Kumar V, Radhakrishnam Raju R, Venkata Reddy R, Chatterjee A, Kiran G, Sridhar G. Amide derivatives of 4-azaindole: Design, synthesis, and EGFR targeting anticancer agents. Synthetic Communications. **2020** Jan 2;50(1):71-84.

16 Meng XY, Zhang HX, Mezei M, Cui M. Molecular docking: a powerful approach for structure-based drug discovery. Current computer-aided drug design. 2011 Jun 1;7(2):146-57.

17 López-Vallejo F, Caulfield T, Martínez-Mayorga K, A Giulianotti M, Nefzi A, A Houghten R, L Medina-Franco J. Integrating virtual screening and combinatorial chemistry for accelerated drug discovery. Combinatorial Chemistry & High Throughput Screening. 2011 Jul 1;14(6):475-87.

18 Huang SY, Zou X. Advances and challenges in protein-ligand docking. International journal of molecular sciences. **2010** Aug 18;11(8):3016-34.

19 Wabdan AK, Mahdi MF, Khan AK. Molecular Docking, Synthesis and ADME Studies of New Pyrazoline Derivatives as Potential Anticancer Agents. Egyptian Journal of Chemistry. **2021** Aug 1; 64(8):4311-22.

20 Bashandy MS. 1-(4-(Pyrrolidin-1-ylsulfonyl) phenyl) ethanone in Heterocyclic Synthesis: Synthesis, Molecular Docking and Anti-Human Liver Cancer Evaluation of Novel Sulfonamides Incorporating Thiazole, Imidazo [1, 2-a] pyridine, Imidazo [2, 1-c][1, 2, 4] triazole, Imidazo [2, 1-b] thiazole, 1, 3, 4-Thiadiazine and 1, 4-Thiazine Moieties. International Journal of Organic Chemistry. **2015**; 5(03):166.

21 Al-Hokbany NS, Alotaibi B, Bin Amer S, Okarvi SM, Al-Jammaz I. Synthesis and In Vitro and In Vivo Evaluation of a New 68Ga-Semicarbazone Complex: Potential PET Radiopharmaceutical for Tumor Imaging. Journal of Chemistry. 2014 Jan 1; 2014.

22 Khidre RE, El-Gogary SR, Mostafa MS. Design, synthesis, and antimicrobial evaluation of some novel pyridine, coumarin, and thiazole derivatives. Journal of Heterocyclic Chemistry. **2017** Jul; 54(4):2511-9.

23 Daina A, Zoete V. A boiled-egg to predict gastrointestinal absorption and brain penetration of small molecules. ChemMedChem. 2016 Jun 6;11(11):1117.

24 Daina A, Michielin O, Zoete V. SwissADME: a free web tool to evaluate pharmacokinetics, drug-likeness and medicinal chemistry friendliness of small molecules. Scientific reports. **2017** Mar 3;7(1):1-3.

25 Jones G, Willett P, Glen RC, Leach AR, Taylor R. Development and validation of a genetic algorithm for flexible docking. Journal of molecular biology. 1997 Apr 4;267(3):727-48

26 Park JH, Liu Y, Lemmon MA, Radhakrishnan R. Erlotinib binds both inactive and active conformations of the EGFR tyrosine kinase domain. Biochemical Journal. **2012** Dec 12;448(Pt 3):417.

27 Dhawan S, Kerru N, Awolade P, Singh-Pillay A, Saha ST, Kaur M, Jonnalagadda SB, Singh P. Synthesis, computational studies and anti-proliferative activities of coumarin-tagged 1, 3, 4-oxadiazole conjugates against MDA-MB-231 and MCF-7 human breast cancer cells. Bioorganic & medicinal chemistry. **2018** Nov 15;26(21):5612-23.

28 Lipinski CA, Lombardo F, Dominy BW, Feeney PJ. Experimental and computational approaches to estimate solubility and permeability in drug discovery and development settings. Advanced drug delivery reviews. **1997** Jan 15;23(1-3):3-25.

29 Allawi MM, Mahdi MF, Raauf AM. Synthesis, anti-inflammatory, molecular docking and ADME studies of new derivatives of ketoprofen as cyclooxygenases inhibitor. Al-Mustansiriyah Journal of Pharmaceutical Sciences (AJPS). **2019** Dec 1;19(4):125-39.
30 Palm K, Stenberg P, Luthman K, Artursson P. Polar molecular surface properties predict the intestinal absorption of drugs in humans. Pharmaceutical research. 1997 May;14(5):568-71.
31 Verdonk ML, Cole JC, Hartshorn MJ, Murray CW, Taylor RD. Improved protein–ligand docking using GOLD. Proteins: Structure, Function, and Bioinformatics. **2003** Sep;52(4):609-23.
32 Adeniyi AA, Ajibade PA. Comparing the suitability of autodock, gold and glide for the docking and predicting the possible targets of Ru (II)-based complexes as anticancer agents. Molecules. **2013** Apr;18(4):3760-78

Received: May 15, 2023/ Accepted: June 10, 2023 / Published: June 15, 2023
Citation: Abdulellah, A.K.; Mahdi ,M.F. ; Raauf,A.M.R. Molecular Docking, Design, Synthesis, Characterization and Pharmacological Evaluation of New 2-hydrazinel Oxazole containing moiety as anti-proliferative activity. Revista Bionatura 2023;8 (2) 63. http://dx.doi.org/10.21931/RB/CSS/2023.08.04.10